Biol. Cybernetics 18, 81—89 (1975)

Visual Apparent Motion and Some Preferred Paths in the Rotation Group $SO(3)$

David H. Foster

Imperial College of Science and Technology, Applied Optics Section, Department of Physics, London, Great Britain

Received: July 10, 1974

Abstract

The sequential presentation of two distinct stimulus objects to the visual system will, under certain conditions, induce an apparent-motion effect, called *beta motion*, in which the first object appears to smoothly transform into the second. This study is concerned with the kinds of paths selected by the visual system in effecting beta motion in which the metric structure of the object is preserved throughout. Two schemes are advanced according to which the visual system might operate. The first concentrates upon the manifold M in which the object appears to transform and the second upon the group G of transformations of M onto itself in which the particular transformation describing this motion lie. Under the identification of M with the 2-sphere S^2, each scheme specifies the action-minimizing curves in the rotation group $SO(3)$ for a particular "natural" Riemannian metric. An experiment is described in which a determination is made of the actual paths taken by an object undergoing various rigid-motion beta motions. The results obtained indicate that the visual system behaves more in accordance with the second scheme than with the first. A generalization of this result is briefly discussed.

1. Introduction

If two visually distinct spots of light are presented to the visual system in rapid succession, then, under appropriate conditions, a visual apparent-motion effect occurs in which the first spot appears to move smoothly across into the second (Wertheimer, 1912; Kenkel, 1913; Kolers, 1972). This phenomenon is known as *beta motion* (and also as *phi motion* and *optimal motion*).

Given an arbitrary visual object A and transform $\sigma(A)$ of A, suppose beta motion can be induced between A and $\sigma(A)$. The question then arises as to the precise nature of the path described by the object in going from its initial to final form. If the visual system operates according to variational principles, it will prefer those paths which minimize the *action*, that is, the integral of the kinetic energy. The kinetic energy depends upon the Riemannian metric assigned to the space in which these paths are defined and there are, in fact, two spaces available for consideration: first, the manifold M in which the object undergoing the beta motion appears to transform, and second, the group G of transformations of M onto itself in which the particular transformations describing this motion lie.

In the present study we shall be concerned with *rigid-motion* beta motion, that is, beta motion in which the metric structure of the object is preserved throughout. Both the corresponding configuration space and the group G can then be identified with the Lie group $SO(3)$ of proper rotations of Euclidean 3-space. This, however, does not mean that we get the same motions in M independent of which space we work with, for the metric induced on $SO(3)$ by the "natural" metric on M is not the same as the metric which is "natural" to $SO(3)$ when the latter is viewed as a representation of G. The aim of this study is to determine, experimentally, which of these two spaces is the more appropriate for the modelling of rigid-motion beta motion.

In Section 2, after giving a formal description of beta motion and fixing an appropriate local coordinate system for configuration space, we set out in detail two schemes by which rigid-motion beta motion might be effected, the one scheme based on M and the other on G. In Section 3, we describe an experiment in which the actual paths of a bar object undergoing various rigid-motion beta motions are explored. The technique employed is to introduce a probe object into the path of the motion and then to adjust its position until the path of the composite motion is visually indistinguishable from the original. In Section 4, we discuss the compatibility of the observed data with each of the two schemes, and then, finally, in Section 5, speculate upon the form of beta motion in general.

2. Two Schemes for Rigid-Motion Beta Motion

2.1. *Notation and Definitions*

The organization here is similar to that of Foster (1973a).

Let $\boldsymbol{R}$ denote the reals. Let S^2 be a fixed sphere in $\boldsymbol{R}^3$, centred at the origin and of dimensions large in comparison with those of the eye. Let the eye be located at the centre of S^2. We associate at all times with S^2 a fixed mapping C of S^2 into $\boldsymbol{R}$, the *background field*, which assigns to each point $p \in S^2$, unless otherwise stated, some specified luminance $C(p) \geqq 0$. (Suppose white-light stimuli.) A visual *object* A on S^2 is, at least, a mapping of a non-empty subset U_A of S^2 into $\boldsymbol{R}$ such that $A(p) \geqq 0$ is the luminance of the object at the point $p \in U_A$. Depending upon the occasion, we allow an object A, or more accurately its *domain* U_A, to inherit certain of the natural structure on S^2. We shall be particularly concerned here with the differentiable structure induced on U_A by the standard (C^∞) differentiable structure on S^2 and the metric structure induced on U_A by the metric structure on S^2 arising from the standard Riemannian structure on S^2. When necessary, U_A may be assumed open in the standard topology on S^2.

Let, then, U be a fixed open subset of S^2 and let $\mathrm{Diff}(U, S^2)$ denote the set of all diffeomorphisms σ taking U onto an open subset $\sigma(U)$ in S^2. We define the action of such a transformation $\sigma \in \mathrm{Diff}(U, S^2)$ on the set $F(U)$ of all objects with domain U by setting

$$(\sigma(A))(p) = A(\sigma^{-1}(p)) \text{ for all } A \in F(U) \text{ and } p \in \sigma(U),$$

which assigns to each point p in the domain of the transformed object $\sigma(A)$ the luminance at its pre-image.

It will be convenient to consider beta motion as if it occurs on S^2. Provided all sets, mappings, and the like defined on S^2 are understood to be specified only to within visual indistinguishability (Zeeman, 1962), the internal subjective phenomenon may certainly be replaced by an equivalent external real motion. Accordingly, if F denotes the set $\cup\{F(V): V \subset S^2\}$ consisting of all objects on S^2, given the sequential presentation to the visual system of some object A and some transform $\sigma(A)$ of A, $\sigma \in \mathrm{Diff}(U_A, S^2)$, *beta motion* between A and $\sigma(A)$ is the generation by the visual system of a smooth time-parametrized curve ω in F joining these two objects. It is a smooth curve in the sense that we consider it arising from the action of a 1-parameter family of transformations $\psi: [0, 1] \times U_A \to S^2$ (see Appendix 1) satisfying $\psi_0(p) = p$ and $\psi_1(p) = \sigma(p)$ for all $p \in U_A$, where ψ_t denotes the mapping $p \in U_A \to \psi(t, p) \in S^2$. Thus,

$$\omega : t \in [0, 1] \to \psi_t(A) \in F .$$

We shall sometimes refer to A as the *initial object* and to $\sigma(A)$ as the *final object*. The symbol σ will always be reserved for the corresponding transformation.

As was said in the Introduction, the interest here is in beta motion that preserves the metric structure of the object throughout. Since objects are defined on S^2, it follows that each transformation ψ_t must coincide with the restriction of a transformation drawn from the orthogonal group $O(3)$. Since, for each $t \in [0, 1]$, ψ_t can be joined to the identity transformation by a smooth curve, we need only consider the identity component of $O(3)$, that is, the rotation group $SO(3)$.

It will be recalled that the *configuration space* of a system is a manifold which models the totality of all its possible positions. For non-trivial objects A on S^2, it is obviously $SO(3)$: we just identify A with the identity I of $SO(3)$.

2.2 *A Local Coordinate System for Configuration Space*

We fix a chart in $SO(3)$ at the identity I with the introduction of canonical coordinates of the second kind. Let x, y, z be the coordinate system of $\boldsymbol{R}^3$, and suppose that the visual axis coincides with the z-axis (and, for later reference, suppose also that the y-axis is vertical). Let $\boldsymbol{SO}(3)$ be the Lie algebra of $SO(3)$ and $\exp : \boldsymbol{SO}(3) \to SO(3)$ the exponential mapping. In matrix representation, we have that

$$L_1 = \begin{pmatrix} 0 & 0 & 0 \\ 0 & 0 & -1 \\ 0 & 1 & 0 \end{pmatrix}, \quad L_2 = \begin{pmatrix} 0 & 0 & 1 \\ 0 & 0 & 0 \\ -1 & 0 & 0 \end{pmatrix},$$

$$L_3 = \begin{pmatrix} 0 & -1 & 0 \\ 1 & 0 & 0 \\ 0 & 0 & 0 \end{pmatrix}$$

form a basis for $\boldsymbol{SO}(3)$. The mapping

$$(\theta_1, \theta_2, \theta_3) \in \boldsymbol{R}^3 \to \exp\theta_1 L_1 \exp\theta_2 L_2 \exp\theta_3 L_3 \in SO(3),$$

which associates with each point $(\theta_1, \theta_2, \theta_3)$

1) a rotation about the z-axis by θ_3,
2) a rotation about the y-axis by θ_2,
3) a rotation about the x-axis by θ_1,

is a diffeomorphism onto its image when restricted to $(-\pi, \pi) \times (-\pi/2, \pi/2) \times (-\pi, \pi)$. This gives us the desired chart at I. We denote the coordinate functions by $\theta_1, \theta_2, \theta_3$. [The matrix representation of the transfor-

mation ϱ with coordinates $(\theta_1(\varrho), \theta_2(\varrho), \theta_3(\varrho))$ is given in Appendix 2.]

In the experiment to be described, the initial object A is a small bar of length 0.015, centred at the point (0, 0, 1) (where S^2 has unit radius). In selecting the transformation σ to fix the final objects $\sigma(A)$, we therefore restrict the range of the coordinate $\theta_3(\sigma)$ to $(-\pi/2, \pi/2)$. The ranges of the other two coordinates $\theta_1(\sigma)$ and $\theta_2(\sigma)$ are each restricted to $(-\varepsilon, \varepsilon)$, $\varepsilon = 0.02$.

2.3. *The Two Schemes*

Before setting up the two schemes for beta motion, we summarize some facts concerning action-minimizing curves in manifolds (see Milnor, 1963; Bishop and Crittenden, 1964).

Let N be a connected complete Riemannian manifold with metric g. Let p and q be any two distinct points of N and let $\Omega(p, q)$ be the set of all smooth curves $\gamma:[0, 1] \to N$ joining p to q. The *action* $S(\gamma)$ of γ is defined by

$$S(\gamma) = \frac{1}{2} \int_0^1 g(\dot{\gamma}(t), \dot{\gamma}(t)) dt ,$$

where $\dot{\gamma}(t)$ is the vector tangent to γ at $\gamma(t)$. The function S achieves its minimum value precisely on the set of *minimizing* geodesics in $\Omega(p, q)$. (A geodesic is *minimizing* if its length is less than or equal to the length of any other piecewise-smooth curve joining its endpoints.) The completeness and connectedness of N guarantee the existence of at least one such geodesic γ_0 in $\Omega(p, q)$. Provided q is not a *cut point* of p along γ_0, so that there is a proper extension of γ_0 beyond q that is still minimizing, this geodesic is also unique. The restrictions on the range of the coordinates $(\theta_1(\sigma), \theta_2(\sigma), \theta_3(\sigma))$ of the transformation σ (Section 2.2) are sufficient to ensure that this uniqueness condition is satisfied in the present cases.

We now proceed with the two schemes, obtaining in each explicit descriptions of the geodesics.

Scheme 1. The object of importance here is the manifold $M = S^2$. It has the natural (standard) Riemannian metric $\langle , \rangle$ obtained by restricting the form $(dx)^2 + (dy)^2 + (dz)^2$ to S^2. For a given object B on S^2, the metric g_1 on $SO(3)$ corresponding to $\langle , \rangle$ is defined in the following way. Let $\varrho \in SO(3)$ and let $X, Y \in T_\varrho SO(3)$, the tangent space to $SO(3)$ at ϱ. For $p \in U_B$, $X(p)$ and $Y(p)$ are in $T_{\varrho(p)} S^2$, the tangent space to S^2 at $\varrho(p)$. Set

$$g_1(X, Y) = \int_{U_B} [X(p), Y(p)]_{\varrho(p)} ds(p) , \qquad (1)$$

where ds is the usual surface measure. Note that, in general, this is a left- but not right-invariant metric.

Now consider the transformation σ. Let $\gamma:[0, 1] \to SO(3)$ be the unique minimizing geodesic (with respect to g_1) joining the identity I to σ. Provided the first two coordinates $\theta_1(\sigma), \theta_2(\sigma)$ of σ and the dimensions of the object A are all small, which is the case here (Section 2.2), then, to a good approximation (see Appendix 3), γ is given in terms of the local coordinate system $\theta_1, \theta_2, \theta_3$ by

$$\begin{aligned} \theta_1(t) &= \theta_1(\sigma) t , \\ \theta_2(t) &= \theta_2(\sigma) t , \\ \theta_3(t) &= \theta_3(\sigma) t , \end{aligned} \qquad (2)$$

where $\theta_i(t) = \theta_i(\gamma(t))$.

Scheme 2. The object of importance here is the group $G = SO(3)$. We assign to it a Riemannian metric g_2 that is invariant under both left and right translations. Such a metric exists since $SO(3)$ is compact. (It is also unique up to a multiplicative factor.) Thus, if $X, Y \in T_I SO(3)$, the tangent space to $SO(3)$ at the identity I, introduce the inner product

$$\text{trace}_I(X Y^*)$$

on $T_I SO(3)$, where Y^* is the transpose of Y, and then extend to all of $SO(3)$ by left translation.

The metric g_2 is natural in that the maximal geodesics with respect to g_2 that pass through I are precisely the 1-parameter subgroups of $SO(3)$. Thus, if $\gamma:[0, 1] \to SO(3)$ is the unique minimizing geodesic (with respect to g_2) joining I to σ, then there exist $\varphi_1, \varphi_2, \varphi_3 \in \boldsymbol{R}$ such that

$$\exp t(\varphi_1 L_1 + \varphi_2 L_2 + \varphi_3 L_3) = \gamma(t) ,$$

where the matrices L_1, L_2, L_3 are defined in Section 2.2. Provided $|\varphi_1|, |\varphi_2| \ll |\varphi_3|$, which is the case here, then, to a good approximation (see Appendix 4), γ is given in terms of the local coordinate system $\theta_1, \theta_2, \theta_3$ by

$$\begin{aligned} \theta_1(t) &= \frac{\varphi_1}{\varphi_3} \sin \varphi_3 t - \frac{\varphi_2}{\varphi_3} (1 - \cos \varphi_3 t) , \\ \theta_2(t) &= \frac{\varphi_1}{\varphi_3} (1 - \cos \varphi_3 t) + \frac{\varphi_2}{\varphi_3} \sin \varphi_3 t , \\ \theta_3(t) &= \varphi_3 t , \end{aligned} \qquad (3)$$

where again $\theta_i(t) = \theta_i(\gamma(t))$.

3. Experiment

To investigate the actual path taken by an object undergoing rigid-motion beta motion, the following experiment was carried out. Two stimulus arrays were

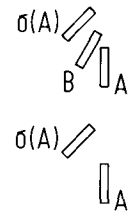

Fig. 1. An example of the full stimulus field

set up as in Fig. 1. The lower array consisted of two fixed bars A, $\sigma(A)$, and the upper array of two fixed bars A, $\sigma(A)$, and a variable probe bar $B = \varrho(A)$, with coordinates $(\theta_1(\varrho), \theta_2(\varrho), \theta_3(\varrho))$. For various values of $\theta_2(\varrho)$, the values of $\theta_1(\varrho)$ and $\theta_3(\varrho)$ were adjusted so that, as point sets, the beta motion induced by the sequential presentation of A, B, $\sigma(A)$ in the upper array visually matched that induced by the sequential presentation of A, $\sigma(A)$ in the lower array.

To quantify the tendency of the recorded points to fit with the curves of the one scheme or the other, a linear regression analysis was performed.

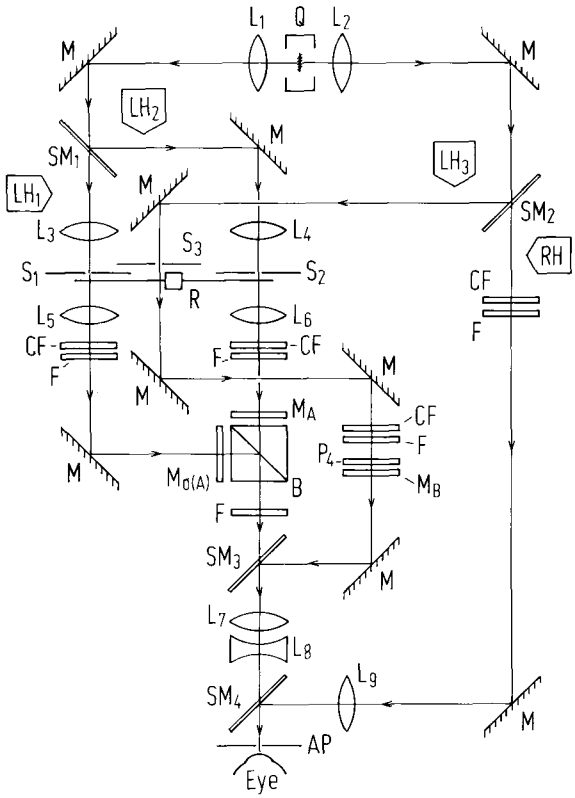

Fig. 2. The experimental apparatus: Q light source; $L_1, L_2, \ldots, L_9$ lenses; M mirrors; SM_1, SM_2, SM_3, SM_4 beam splitting mirrors; S_1, S_2, S_3 stops: CF colour-correcting filters; F neutral density filters; R sector; P_4 polaroid sheet; M_A, $M_{\sigma(A)}$, M_B masks; B beam splitter cube; AP artificial pupil

3.1. Apparatus

A diagram of the apparatus, which is a modification of that used in an earlier study (Foster, 1973b), is shown in Fig. 2. It consisted essentially of four channels, each forming a Maxwellian view system. Channels LH_1, LH_2, and LH_3 gave rise to the various test stimuli and channel RH to the uniform background field.

The single light source Q was a 12 V, 100 W quartz-iodine lamp with a compact coiled filament. It was run from a stabilized power supply which maintained fluctuations in the light level to within 0.25% of the mean. Light was taken from both sides of Q and collimated by the lenses L_1 and L_2. The left hand beam was divided (amplitude division in all cases) by the beam splitting mirror SM_1 and the two resulting beams focussed by the lenses L_3 and L_4 onto the stops S_1 and S_2. The light was then recollimated by the lenses L_5 and L_6. The parallel light beam is channel LH_1 transilluminated the mask $M_{\sigma(A)}$ and that in channel LH_2 the mask M_A. The two beams were brought together by the beam splitter cube B. The right hand beam was divided by the beam splitting mirror SM_2. The parallel light beam in channel LH_3 after passing through aperture S_3 (located above S_1 and S_2) transilluminated the mask M_B. The beam was then combined with the beams from LH_1 and LH_2 by the beam splitting mirror SM_3, after which all three beams were brought to a focus at the 2 mm artificial pupil AP by the lenses L_7 and L_8. The parallel light beam in channel RH was brought to a focus at AP by the lens L_9 and the beam splitting mirror SM_4. The pupil was completely filled with light.

With the colour-correcting filters CF and neutral density filters F in place, the channels LH_1, LH_2, LH_3, and RH all matched in colour and brightness from SM_4 onwards.

The masks M_A, $M_{\sigma(A)}$, and M_B defined the corresponding objects in the two test arrays and examples are shown in Fig. 3a. The mask M_B was mounted in a cylindrical bearing fixed on an adjustable table, which allowed precise and independent control of the orientation $\theta_3(\varrho)$ and position $\theta_1(\varrho)$, $\theta_2(\varrho)$ of the probe object.

The construction of the sector R is shown in Fig. 3b. The two "open" sections were covered by polaroid sheets P_1 and P_2, with the axis of P_1 perpendicular to that of P_2. The axes of the polaroid sheets P_3 and P_4 covering the top aperture in $M_{\sigma(A)}$ and the single aperture of M_B (Fig. 2) were also perpendicular. When the sector R rotated, the stimuli appeared in the order indicated in Fig. 4.

The full test field shown in Fig. 1 is to scale. Corresponding points in the two arrays subtended 2.7° at the eye, the long side of each bar subtended 0.9°, and the background field (not shown) subtended 11°. The retinal illumination of each bar was 4800 trolands and that of the background field was 2400 trolands. The colour temperature was 3200 °K.

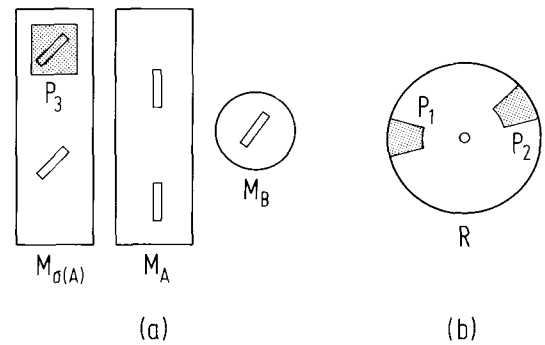

Fig. 3a and b. Examples of the masks M_A, $M_{\sigma(A)}$, M_B, and the sector R: P_1, P_2, P_3 are polarized sheets

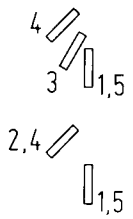

Fig. 4. The order of presentation of the component stimuli of Fig. 1

3.2. Procedure

Only those pairs of masks M_A, $M_{\sigma(A)}$ for which rigid-motion beta motion could be induced were used. The period of the stimulus cycle (Fig. 4) was set at 2.0 sec.

The subject, equipped with a dental bite-bar, monocularly fixated the centre of either the top or bottom array. The horizontal position $\theta_2(\varrho)$ of the probe bar B was fixed by the experimenter so that $0 \leqq \theta_2(\varrho) \leqq \theta_2(\sigma)$. The subject then adjusted the vertical position $\theta_1(\varrho)$ and orientation $\theta_3(\varrho)$ of B so that as point sets (i.e., with no reference to time parametrization) the resultant beta motion of the top array was visually indistinguishable from that of the bottom array. There was no limit on observation time.

The coordinate $\theta_2(\varrho)$ was reset by the experimenter and the above procedure repeated. The probe bar B was in this way tracked from one end of the top display to the other and then back a total of four times. At each value of $\theta_2(\varrho)$ eight determinations of $\theta_1(\varrho)$ and $\theta_3(\varrho)$ were thus obtained. The beta motion associated with seven different pairs of patterns A, $\sigma(A)$ was investigated.

Two subjects were employed: FMF, who was myopic and aged twenty-six years, and DHF (the author), who was myopic and aged twenty-eight years. In both cases, the apparent distance of the test stimuli was within the range of accommodation of the subject's naked eye. FMF was unaware of the purpose of the study.

3.3. Analysis of Data

A linear regression analysis was carried out (see, for example, Draper and Smith, 1966).

The Schemes 1 and 2 imply respective dependencies upon $\theta_2(\varrho)$ of the expected value $E(\theta_i(\varrho))$ of $\theta_i(\varrho)$, $i = 1, 3$, thus:

$$E(\theta_i(\varrho)) = f_i(\theta_2(\varrho)),$$
$$E(\theta_i(\varrho)) = g_i(\theta_2(\varrho)),$$

where the functions f_i and g_i are defined implicitly by (2) and (3) respectively. The true experimental curves must pass through the fixed end-points $(0, 0, 0)$ and $(\theta_1(\sigma), \theta_2(\sigma), \theta_3(\sigma))$, be smooth, and, we suppose, be like f_i and g_i in the following sense:

$$E(\theta_i(\varrho)) = w_i g_i(\theta_2(\varrho)) + (1 - w_i) f_i(\theta_2(\varrho)), \tag{4}$$

where $-\infty < w_i < \infty$. If Scheme 1 holds, then $w_i = 0$, and if Scheme 2 holds, then $w_i = 1$.

The ordinary least squares estimate w_i' of the regression coefficient w_i is given by

$$w_i' = \frac{\sum_{j=1}^{m} \sum_{k=1}^{n} h_i(\theta_{2;j})(\theta_{i;j,k} - f_i(\theta_{2;j}))}{\sum_{j=1}^{m} \sum_{k=1}^{n} (h_i(\theta_{2;j}))^2},$$

where $h_i = g_i - f_i$, m is the number of distinct values $\theta_{2;j}$ assigned to the variable $\theta_2(\varrho)$, and n is the fixed number (eight) of determinations $\theta_{i;j,k}$ of $\theta_i(\varrho)$ at each $\theta_{2;j}$. The estimated standard error s_i of w_i' is given by

$$s_i^2 = \frac{\sum_{j=1}^{m} \sum_{k=1}^{n} (\theta_{i;j,k} - \theta_{i;j}')^2}{(N-1) \sum_{j=1}^{m} \sum_{k=1}^{n} (h(\theta_{2;j}))^2},$$

where $\theta_{i;j}' = w_i' g_i(\theta_{2;j}) + (1 - w_i') f_i(\theta_{2;j})$ and $N = mn$. A $100(1-\alpha)\%$ confidence interval $[u_i, v_i]$ for w_i is then

$$[u_i, v_i] = [w_i' - t_{N-1,1-\alpha/2} s_i, w_i' + t_{N-1,1-\alpha/2} s_i],$$

where $t_{N-1,1-\alpha/2}$ is the $(1-\alpha/2)$ % point of a t-distribution with $N-1$ degrees of freedom.

The adequacy of the statistical model underlying (4) is tested by comparing the "lack of fit" sum of squares with the pure error sum of squares. We compute the ratio

$$F_i = \frac{\left[\sum_{j=1}^{m} n(\bar{\theta}_{i;j} - \theta_{i;j}')^2\right] \Big/ (m-1)}{\left[\sum_{j=1}^{m} \sum_{k=1}^{n} (\theta_{i;j,k} - \bar{\theta}_{i;j})^2\right] \Big/ (N-m)},$$

where $\bar{\theta}_{i;j} = \frac{1}{n} \sum_{k=1}^{n} \theta_{i;j,k}$. If the ratio is significant, that is, if F_i exceeds $F_{m-1,N-m,1-\alpha}$, the $100(1-\alpha)\%$ point of an F distribution with $m-1$ and $N-m$ degrees of freedom, the model is rejected.

In both determining confidence intervals for w_i and testing the adequacy of the model we work at the level $\alpha = 0.01$.

In those cases in which the model is accepted, we distinguish two particular outcomes:

$$u_i \leqq 0 \leqq v_i < 1, \tag{5}$$

$$0 < u_i \leqq 1 \leqq v_i. \tag{6}$$

We take (5) as support for Scheme 1 and (6) as support for Scheme 2.

4. Results

The data obtained from the experiments described in Section 3 are plotted in Fig. 5a–h. In each figure, the means of the observed values of the coordinates $\theta_i = \theta_i(\varrho)$, $i = 1, 3$, of the probe object $B = \varrho(A)$ are shown against the selected values of the coordinate $\theta_2 = \theta_2(\varrho)$, with the standard deviations of the observed values marked by vertical lines. In each case, the functions f_i and g_i (Section 3.3) describing the variations with $\theta_2(\varrho)$ of the expected values of the coordinates $\theta_i(\varrho)$, $i = 1, 3$, according to Schemes 1 and 2, are shown by the broken and continuous curves respectively. The points corresponding to the initial and final objects are circled. The values of the constants φ_1, φ_2, φ_3 (Section 2.3) are also given.

It is clear from a superficial inspection of Fig. 5 that there is an overall tendency of the observed beta motion to follow the curves of Scheme 2 rather than

those of Scheme 1. This is particularly evident in Fig. 5c and d in the coordinate θ_1. The results of the formal analysis (Section 3.3), which are summarized in Table 1, provide support for this conclusion. It is seen that there are eight cases in which precisely one of the two schemes is indicated. Of these eight, six give Scheme 2 and only two give Scheme 1. [It is also seen that in only three cases is the statistical model underlying (4) proved inadequate.] In the remaining five cases in which the model is accepted, but neither

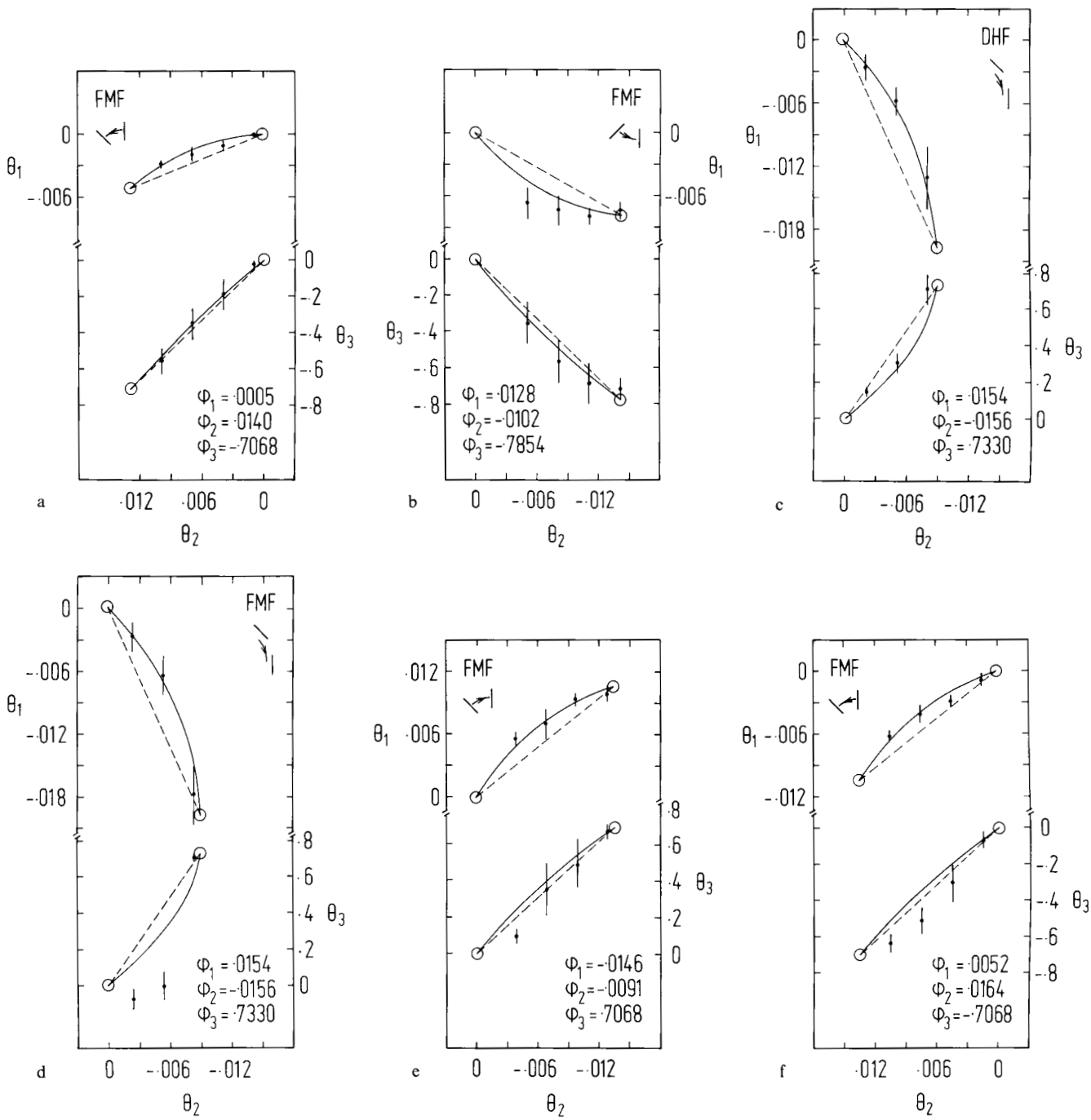

Fig. 5a—h. Means of the recorded values of the coordinates $\theta_i = \theta_i(\varrho)$, $i = 1, 3$, obtained at selected values of the coordinate $\theta_2 = \theta_2(\varrho)$, with associated standard deviations. The continuous curves show the expected values according to Scheme 2 and the broken curves the expected values according to Scheme 1

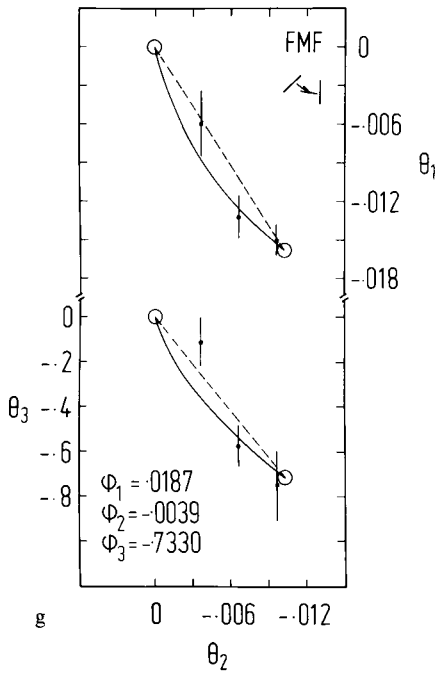

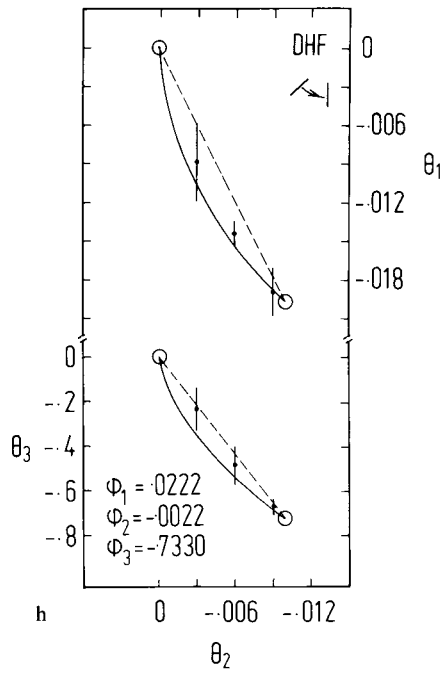

Table 1

Experiment	i	w_i'	F_i	$[u_i, v_i]$	Indicated scheme
(a)	1	0.70	2.05	[0.44, 0.95]	
	3	0.51	0.44	[−1.29, 2.32]	
(b)	1	1.92	1.01	[1.44, 2.41]	
	3	1.80	1.09	[0.32, 3.28]	2
(c)	1	1.17	1.04	[0.82, 1.53]	2
	3	0.30	9.13[a]		
(d)	1	0.87	5.68	[0.48, 1.26]	2
	3	2.42	94.44[a]		
(e)	1	1.05	2.55	[0.67, 1.42]	2
	3	−1.05	1.51	[−2.56, 0.46]	1
(f)	1	0.80	3.47	[0.52, 1.08]	2
	3	−2.41	0.26	[−3.42, −1.40]	
(g)	1	0.47	4.93	[−0.08, 1.02]	
	3	0.48	10.97[a]		
(h)	1	0.69	0.20	[0.31, 1.06]	2
	3	0.23	0.78	[−0.12, 0.72]	1

[a] Significant.

scheme is uniquely indicated, no common value of the regression coefficient w_i is evidenced. The possibility that the form of the initial object is of importance in determining the final motion cannot of course be ruled out, but the investigation of this is not within the scope of the present study.

5. Discussion

We have constructed two schemes according to which the visual system might effect rigid-motion beta motion between two objects on the sphere S^2. The first specifies the action-minimizing curves in the associated configuration space, that is, $SO(3)$, when equipped with the metric corresponding to the standard Riemannian metric on S^2, and the second specifies the action-minimizing curves in the group of rigid motions of S^2, that is, $SO(3)$, when equipped with a bi-invariant Riemannian metric. The results of the experimentation imply that at least for the pairs of objects considered the visual system behaves more in accordance with the second scheme than with the first.

Consider, now, the case of general beta motion. For each domain $U \subset S^2$, suppose that the set consisting of all local transformations of S^2 which have domain U and which the visual system is capable of effecting through beta motion forms a local Lie transformation group $G \times U \to S^2$, where G is a local Lie group. Thus, if $\iota: G \to \mathrm{Diff}(U, S^2)$ is the canonical injection, we have for any beta motion, ψ_t, $t \in [0, 1]$, a commutative diagram

$$\begin{array}{ccc} [0,1] & \xrightarrow{t \to \psi_t} & \mathrm{Diff}(U, S^2) \\ & {\scriptstyle\gamma}\searrow \quad \nearrow{\scriptstyle\iota} & \\ & G & \end{array}$$

for some path $\gamma: [0, 1] \to G$ with $\gamma(0) = e$, the identity of G. In view of the outcome of the present study, it is

natural to conjecture that the path γ lies on a local 1-parameter subgroup in G. If this conjecture is valid, then the family ψ_t must be the restriction to $[0, 1]$ of a local 1-parameter group of local transformations, so that if s, t, $s+t \in [0, 1]$ and if p, $\psi_t(p) \in U$, then

$$\psi_{s+t}(p) = \psi_s(\psi_t(p)) . \tag{7}$$

This property should not be difficult to check experimentally for an observed family ψ_t, since (7) is precisely the condition for "steady flow", that is, the invariance of the velocity field of the flow ψ_t by the flow. It is easy to see that whereas the second scheme of this study always gives flows which are steady, the first sometimes gives flows which are not.

Acknowledgements. The author wishes to thank Dr. C. J. Isham and Mr. R. Rutstein for much useful advice and discussion, and for critical readings of the manuscript.

Appendix 1 (Section 2.1)

A *1-parameter family of transformations* defined on an open subset U of S^2 is a differentiable mapping ψ of $[0, 1] \times U$ into S^2 such that for each $t \in [0, 1]$, the mapping $\psi_t : p \to \psi(t, p)$ is a diffeomorphism of U onto $\psi_t(U)$.

Appendix 2 (Section 2.2)

We have, for $\theta_1, \theta_2, \theta_3 \in \boldsymbol{R}$,

$$\exp \theta_1 L_1 = \begin{pmatrix} 1 & 0 & 0 \\ 0 & \cos\theta_1 & -\sin\theta_1 \\ 0 & \sin\theta_1 & \cos\theta_1 \end{pmatrix},$$

$$\exp \theta_2 L_2 = \begin{pmatrix} \cos\theta_2 & 0 & \sin\theta_2 \\ 0 & 1 & 0 \\ -\sin\theta_2 & 0 & \cos\theta_2 \end{pmatrix},$$

$$\exp \theta_3 L_3 = \begin{pmatrix} \cos\theta_3 & -\sin\theta_3 & 0 \\ \sin\theta_3 & \cos\theta_3 & 0 \\ 0 & 0 & 1 \end{pmatrix}.$$

The matrix representation of the transformation ϱ is by definition $\exp\theta_1 L_1 \exp\theta_2 L_2 \exp\theta_3 L_3$, where $\theta_i = \theta_i(\varrho)$, $i = 1, 2, 3$. By direct evaluation this is

$$\begin{pmatrix} \cos\theta_2\cos\theta_3 & -\cos\theta_2\sin\theta_3 & \sin\theta_2 \\ \cos\theta_1\sin\theta_3 + \sin\theta_1\sin\theta_2\cos\theta_3 & \cos\theta_1\cos\theta_3 - \sin\theta_1\sin\theta_2\sin\theta_3 & -\sin\theta_1\cos\theta_2 \\ \sin\theta_1\sin\theta_3 - \cos\theta_1\sin\theta_2\cos\theta_3 & \sin\theta_1\cos\theta_3 + \cos\theta_1\sin\theta_2\sin\theta_3 & \cos\theta_1\cos\theta_2 \end{pmatrix}.$$

Appendix 3 (Section 2.3)

The metric g_1 is invariant under left translations $L_\tau : \tau' \in SO(3) \to \tau\tau' \in SO(3)$, $\tau \in SO(3)$. In particular, for X, $Y \in T_\sigma SO(3)$,

$$g_1(X, Y) = g_1((L_{\sigma^{-1}})_* X, (L_{\sigma^{-1}})_* Y) \tag{A1}$$

where $(L_{\sigma^{-1}})_*$ is the induced mapping of the tangent spaces. Since $(L_{\sigma^{-1}})_* X$, $(L_{\sigma^{-1}})_* Y \in T_I SO(3)$, we can find a_i, $b_j \in \boldsymbol{R}$, $i, j = 1, 2, 3$, such that

$$(L_{\sigma^{-1}})_* X = \sum_{i=1}^{3} a_i L_i \quad \text{and} \quad (L_{\sigma^{-1}})_* Y = \sum_{j=1}^{3} b_j L_j .$$

Suppose, without loss in generality, that the initial object A is oriented with its long axis parallel to the y-axis. Let l_1 and l_2 be the width and length of A respectively. Evaluating the right side of (1) for A, we get

$$\begin{aligned} g_1((L_{\sigma^{-1}})_* X, (L_{\sigma^{-1}})_* Y) = {} & \tfrac{1}{2}(a_2 b_2 + a_3 b_3) l_1 (l_2 - \sin l_2) \\ & + \tfrac{1}{2}(a_3 b_3 + a_1 b_1) l_2 (l_1 - \sin l_1) \\ & + \tfrac{1}{2}(a_1 b_1 + a_2 b_2)(l_1 \sin l_2 + l_2 \sin l_1) . \end{aligned} \tag{A2}$$

Let $\gamma : [0, 1] \to SO(3)$ be an arbitrary smooth curve with $\gamma(0) = I$ and $\gamma(1) = \sigma$, lying entirely within the coordinate neighbourhood of I. The kinetic energy $T(\dot\gamma(t))$ of γ at the point $\gamma(t)$ is, by definition, $\frac{1}{2} g_1(\dot\gamma(t), \dot\gamma(t))$. Suppose for some $c_i : [0, 1] \to \boldsymbol{R}$, $i = 1, 2, 3$,

$$(L_{\gamma(t)^{-1}})_* \dot\gamma(t) = \sum_{i=1}^{3} c_i(t) L_i .$$

Let $\gamma(t)$ have coordinates $(\theta_1(t), \theta_2(t), \theta_3(t))$. Then, using the expression given in Appendix 2, we obtain

$$\begin{aligned} c_1(t) &= \cos\theta_3(t)\cos\theta_2(t)\dot\theta_1(t) + \sin\theta_3(t)\dot\theta_3(t) , \\ c_2(t) &= -\sin\theta_3(t)\cos\theta_2(t)\dot\theta_1(t) + \cos\theta_3(t)\dot\theta_2(t) , \\ c_3(t) &= \dot\theta_3(t) + \sin\theta_2(t)\dot\theta_1(t) . \end{aligned}$$

From (A1) and (A2) we then get the following for the local representative T' of T

$$T'(\theta_1(t), \ldots, \dot\theta_3(t)) = \tfrac{1}{2}[l_1 l_2((\dot\theta_1(t))^2 + (\dot\theta_2(t))^2) + 1/12(l_1^2 + l_2^2)(\dot\theta_3(t))^2] ,$$

where we have ignored higher order terms in l_1, l_2, $\theta_1(t)$, $\theta_2(t)$ (each of the last having magnitude not greater that 0.02). For γ to be a geodesic it must satisfy Lagrange's equations

$$\frac{d}{dt}\left[\frac{\partial T'}{\partial \dot\theta_i}(\theta_1(t), \ldots, \dot\theta_3(t))\right] = \frac{\partial T'}{\partial \theta_i}(\theta_1(t), \ldots, \dot\theta_3(t)) ,$$

$i = 1, 2, 3$. In this case, $\dot\theta_i(t) =$ constant, and so $\theta_i(t) = \theta_i(\sigma)t$, $i = 1, 2, 3$.

Appendix 4 (Section 2.3)

For $\varphi_1, \varphi_2, \varphi_3 \in \boldsymbol{R}$, let φ denote the matrix

$$\varphi_1 L_1 + \varphi_2 L_2 + \varphi_3 L_3 = \begin{pmatrix} 0 & -\varphi_3 & \varphi_2 \\ \varphi_3 & 0 & -\varphi_1 \\ -\varphi_2 & \varphi_1 & 0 \end{pmatrix}.$$

The (r, s)th element in the product φ^{2n}, n a positive integer, is given by the following formula.

$$(\varphi^{2n})_{rs} = \left(\sum_{i=1}^{3} \varphi_i^2\right)^{n-1} (-1)^{n-1} \left(\varphi_r \varphi_s - \delta_{rs} \sum_{i=1}^{3} \varphi_i^2\right),$$

where δ_{rs} is the Kronecker delta.

By writing

$$\exp t\varphi = \sum_{n=0}^{\infty} \frac{(t\varphi)^{2n}}{(2n)!} + t\varphi \cdot \sum_{n=0}^{\infty} \frac{(t\varphi)^{2n}}{(2n+1)!} , \quad 0 \leqq t \leqq 1 ,$$

and making use of the above formula we obtain

$$\begin{aligned} (\exp t\varphi)_{rs} = {} & \delta_{rs} + t(\varphi)_{rs} + (\varphi_r \varphi_s - \delta_{rs} p^2)\left[\frac{1 - \cos pt}{p^2}\right] \\ & + \sum_{j=1}^{3} (\varphi)_{rj}(\varphi_j \varphi_s - \delta_{js} p^2)\left[\frac{pt - \sin pt}{p^3}\right], \end{aligned}$$

where $p^2 = \sum_{i=1}^{3} \varphi_i^2$. Ignoring second order terms in φ_1, φ_2 (each having magnitude less than 0.025, the magnitude of φ_3 being greater than 0.7), we then get

$$\exp t\varphi = \begin{pmatrix} \cos\varphi_3 t & -\sin\varphi_3 t & \frac{\varphi_1}{\varphi_3}(1-\cos\varphi_3 t) + \frac{\varphi_2}{\varphi_3}\sin\varphi_3 t \\ \sin\varphi_3 t & \cos\varphi_3 t & \frac{\varphi_2}{\varphi_3}(1-\cos\varphi_3 t) - \frac{\varphi_1}{\varphi_3}\sin\varphi_3 t \\ \frac{\varphi_1}{\varphi_3}(1-\cos\varphi_3 t) - \frac{\varphi_2}{\varphi_3}\sin\varphi_3 t & \frac{\varphi_2}{\varphi_3}(1-\cos\varphi_3 t) + \frac{\varphi_1}{\varphi_3}\sin\varphi_3 t & 1 \end{pmatrix}.$$

Direct comparison of this with the matrix having coordinates $(\theta_1(t), \theta_2(t), \theta_3(t))$ given in Appendix 2 yields

$$\theta_1(t) = \frac{\varphi_1}{\varphi_3}\sin\varphi_3 t - \frac{\varphi_2}{\varphi_3}(1-\cos\varphi_3 t),$$

$$\theta_2(t) = \frac{\varphi_1}{\varphi_3}(1-\cos\varphi_3 t) + \frac{\varphi_2}{\varphi_3}\sin\varphi_3 t,$$

$$\theta_3(t) = \varphi_3 t,$$

where higher order terms in φ_1, φ_2 have again been ignored.

References

Bishop, R., Crittenden, R.: Geometry of manifolds. New York: Academic Press 1964

Draper, N.R., Smith, H.: Applied regression analysis. New York: Wiley 1966

Foster, D.H.: A hypothesis connecting visual pattern recognition and apparent motion. Kybernetik **13**, 151—154 (1973a)

Foster, D.H.: An experimental examination of a hypothesis connecting visual pattern recognition and apparent motion. Kybernetik **14**, 63—70 (1973b)

Kenkel, F.: Untersuchungen über den Zusammenhang zwischen Erscheinungsgröße und Erscheinungsbewegung bei einigen sogenannten optischen Täuschungen. Z. Psychol. **67**, 358—449 (1913)

Kolers, P.A.: Aspects of motion perception. Oxford: Pergamon Press 1972

Milnor, J.: Morse theory, Annals of mathematics studies No. 51. Princeton, N.J.: Princeton University Press 1963

Wertheimer, M.: Experimentelle Studien über das Sehen von Bewegung. Z. Psychol. **61**, 161—265 (1912)

Zeeman, E.C.: The topology of the brain and visual perception. In: The topology of 3-manifolds and related topics. New Jersey: Prentice-Hall 1962

Dr. D. H. Foster
Imperial College of Science
and Technology
Dept. of Physics
Prince Consort Road
London SW7 2BZ, Great Britain